Electron transport through metal/MoS_2 interfaces: edge- or area-dependent process?

Áron Szabó[†], Achint Jain[‡], Markus Parzefall[‡],

Lukas Novotny[‡], and Mathieu Luisier[†*]

[†] *Integrated System Laboratory, ETH Zürich, 8092 Zürich, Switzerland*

[‡] *Photonics Laboratory, ETH Zürich, 8093 Zürich, Switzerland*

E-mail: mluisier@iis.ee.ethz.ch

Phone: +41 44 632 53 33. Fax: +41 44 632 11 94

Construction of the Device Hamiltonian Matrices from DFT

The method to construct the metal-(oxide)-semiconductor structures and the corresponding Hamiltonian matrices are described in great details in Appendix B of Ref.[1] The most important steps are summarized here for convenience. To accurately simulate electronic transport through contact heterojunctions, large atomic systems must be treated at the density functional theory (DFT) level, which is not directly possible with plane-wave codes such as VASP.[2] This is why we had to come up with the method proposed below.

Here, we focus on the metal-semiconductor configuration, but the developed approach applies to the case with oxide inbetween as well. The first step consists in identifying a common periodic unit cell that contains both the metal, Mo, and S atoms. It has been demonstrated before that a thickness of 6 atomic layers is sufficient to describe the electronic properties of a top metal

*To whom correspondence should be addressed

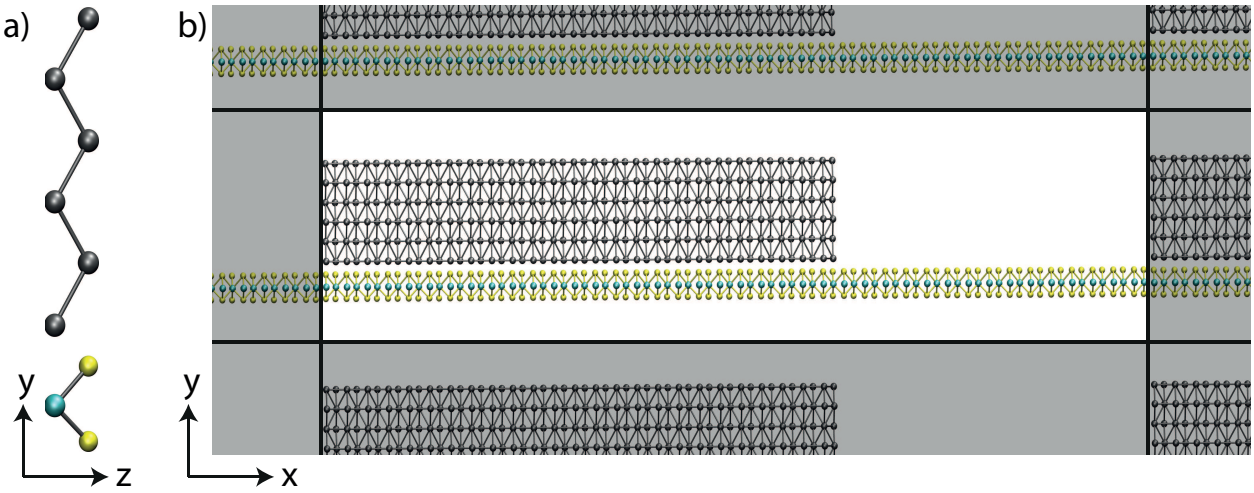

Figure S1: (a) Side view of the atoms in the created primitive cell of the metal-MoS_2 heterostructure. Cyan dots denote Mo atoms, yellow S, and gray metal. (b) The area in the center with the white background represents the unit cell of MoS_2 with a top metal contact. It is made of 576 atoms and is simulated at the DFT level. Shaded regions refer to periodic replicas.

electrode.[3] Hence, 6 Ti layers were placed above MoS_2. The unit cell of the compound system is depicted in Fig. S1(a). The distance between the top S and bottom Ti atoms was determined by relaxing all ions within the generated unit cell, except those belonging to the top four metallic layers. A 10 Å vacuum region separates the periodic replicas from each other in the vertical y direction. Van der Waals interactions were included through the DFT-D2 method of Grimme.[4] A $11\times1\times11$ Monkhorst-Pack k-point mesh and a convergence criteria of less than 10^{-3} eV/Å for the forces acting on each atom were set. The vertical separation between the Ti and the semiconductor layer was consistently found to be 1.54 Å, regardless of the initial assumptions. All calculations were performed with VASP[2] on a local cluster.

Using this optimized geometry a rectangular supercell was assembled that contains many replicas of the primitive unit cell along the transport direction x and also a region where the metal atoms were removed so that only the MoS_2 semiconductor layer is present. This cell is displayed in Fig. S1(b). For the considered Ti-MoS_2 system, the central part is composed of 576 atoms. Its electronic structure was computed with VASP, before converting the resulting plane-wave Hamiltonian matrix into a set of maximally localized Wannier functions (MLWFs) with the Wannier90 tool.[5] For that purpose, the Brillouin zone was first sampled with 5 points in the k_z direction at

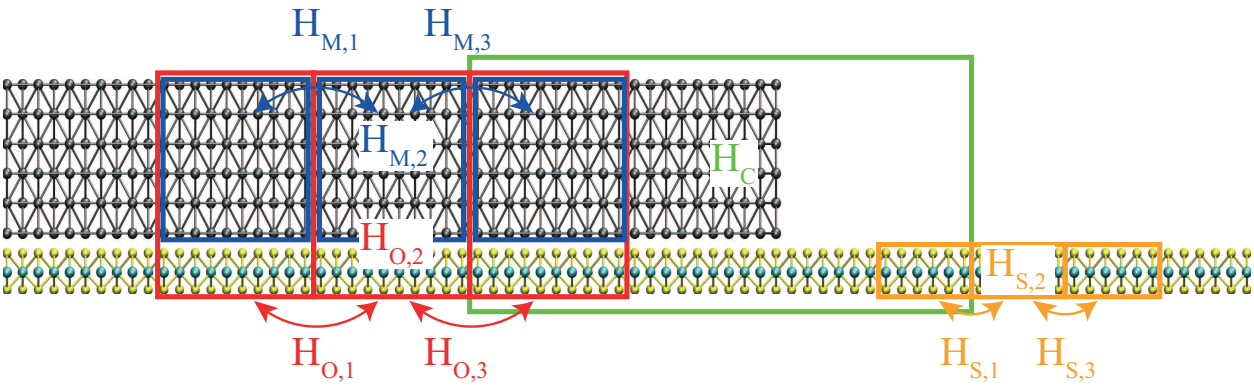

Figure S2: Extraction of the Hamiltonian blocks utilized to construct $\mathbf{H_{MLWF}}$, the Hamiltonian matrix of a device with realistic dimensions. Blue rectangles identify the regions from which interactions between cells containing only metal atoms are taken, red unit cells where the metal and semiconductor parts overlap, and orange the semiconductor-only part. The green rectangle contains the Hamiltonian block that is needed to connect the metal-semiconductor region and the semiconductor-only extension together. Note that all Hamiltonian blocks corresponding to a marked region and to the coupling with their neighbors have been carefully labeled.

k_x=k_y=0 to self-consistently determine the charge density. The number of k_z points was then increased to 9 and the number of bands (NBANDS) to 3600 to recompute the wavefunctions with the charge fixed to its converged value. This step is necessary to facilitate the conversion to MLWFs, in particular to obtain a smoother subspace of bands that can be disentangled from the Hilbert space. As initial projections Mo:l=2, S:l=1, Ti:l=2, and Ti:sp3-1 were supplied to Wannier90. The frozen energy window was selected in such a way that it covers a 2 eV range around the Fermi level, giving rise to well localized Wannier functions.

The idea behind this procedure is that the MLWF Hamiltonian can be broken down in small blocks that can be replicated and re-assembled together in a different way in order to produce the Hamiltonian of a system where the metal and semiconductor parts extend to realistic scales. The method is illustrated in Fig. S2. First, in the region where the metal and the semiconductor overlap, three identical cells are identified, each of them is delimited by a red rectangle. It is important that all atomic interactions that start from the central cell do not extend beyond its left and right neighboring cells. If this condition is satisfied, three Hamiltonian blocks can be extracted for the central cell, one that includes its interactions with its left neighbor, one with itself, and a last one with its right neighbor. They are denoted as $\mathbf{H_{O,1}}$, $\mathbf{H_{O,2}}$, and $\mathbf{H_{O,3}}$, respectively. The same

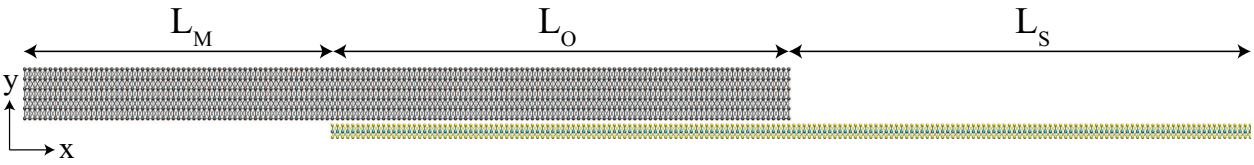

Figure S3: Schematic view of a top metal contact deposited on a MoS_2 monolayer with extended lateral dimensions. In this work, the lengths L_M (pure metal), L_O (overlap region), and L_S (semiconductor-only) measure 10 nm, 6 to 133 nm, and 50 nm, respectively.

procedure can be repeated in the semiconductor-only region, where the cells are colored in orange and the Hamiltonian blocks are denoted as $\mathbf{H_{S,1}}$, $\mathbf{H_{S,2}}$, and $\mathbf{H_{S,3}}$.

The metal-semiconductor overlapping part on the left and the semiconductor-only extension on the right are connected through a Hamiltonian block labeled $\mathbf{H_C}$ that corresponds to the region delimited by a green rectangle in Fig. S2. The off-diagonal block that connects this L-shaped structure to the metal-semiconductor region is $\mathbf{H_{O,1}}$, while the one that couples it to the semiconductor-only region is $\mathbf{H_{S,3}}$. Additionally, another set of three cells must be identified within the overlapping region, namely the metal-only parts, shown in blue. The corresponding Hamiltonian blocks are denoted as $\mathbf{H_{M,1}}$, $\mathbf{H_{M,2}}$, and $\mathbf{H_{M,3}}$. These Hamiltonian components are required to build a pure metal extension on the left side from which electrons can be injected into the simulation domain, as illustrated in Fig. S3. It remains to determine the connection between the rightmost metal-only block and the start of the overlapping region, which is labeled $\mathbf{H_{MO}}$ and is a subset of $\mathbf{H_{O,3}}$. We may ask ourselves whether it is justified to extract the Hamiltonian matrix of a pure Ti layer from that of a Ti-Mo_2 heterojunction. In fact, the electronic states of the metallic layer are only marginally influenced by the presence of a 2-D material underneath so that their properties are not affected. The same cannot be said about the semiconductor layer because the high electron concentration present in the metallic electrode situated above it drastically modifies its bandstructure. This is the reason why the unit cell used in DFT must have a MoS_2-only region.

Taking all the above points into consideration, the Hamiltonian $\mathbf{H_{MLWF}}$ of the system depicted in Fig. S3 can be put together. It is sketched in Fig. S4 with the help of the quantities introduced in Fig. S2. The Hamiltonian blocks containing the interactions between the metal-only parts (blue)

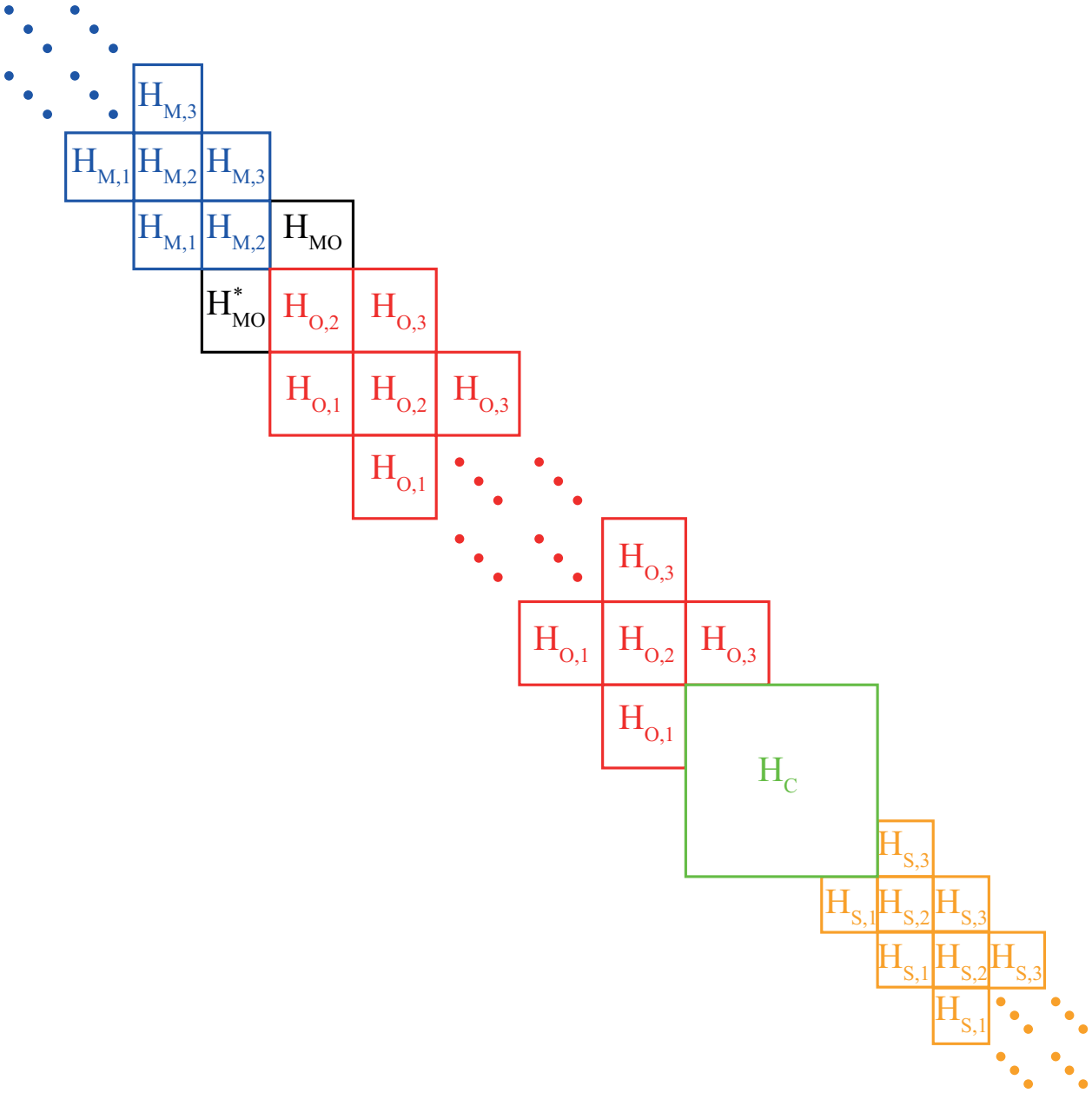

Figure S4: Schematic view of the $\mathbf{H_{MLWF}}$ Hamiltonian matrix corresponding to the device in Fig. S3. The colors and the notations refer to the quantities introduced in Fig. S2.

are repeatedly placed in a tridiagonal fashion first. They are then connected through the $\mathbf{H_{MO}}$ block (black) to the region where the metal and the semiconductor layer overlap (red). The latter part is connected to the semiconductor-only volume (orange) through the central green block.

NEGF Simulation Approach

Once that the MLWF Hamiltonian $\mathbf{H_{MLWF}}$ that corresponds to the desired simulation domain has been assembled, the current that flows through the contact geometry, from the pure metallic region to the MoS_2-only extension can be computed. In this paper, this was done with the well-established Non-equilibrium Green's Function (NEGF) formalism, a powerful quantum transport technique compatible with a MLWF basis set. A computational approach very similar to the one described in Ref.[6] was used. The equations to be solved have the following form

$$\Big(E - \mathbf{H_{MLWF}}(k_z) - \Sigma^{RB}(k_z,E) - \Sigma^{RS}(k_z,E)\Big) \cdot G^R(k_z,E) \quad = \quad I \tag{1}$$

$$G^{\gtrless}(k_z,E) \quad = \quad G^R(k_z,E) \cdot \Big(\Sigma^{\gtrless B}(k_z,E) + \Sigma^{\gtrless S}(k_z,E)\Big) \cdot G^A(k_z,E), \tag{2}$$

In Eqs. (1) and (2), the unknowns are the retarded/advanced $G^{R/A}(k,E)$ and greater/lesser $G^{\gtrless}(k,E)$ Green's functions at energy E and momentum k_z. They are full matrices of size $N_A \times N_{WF}$ where N_A is the number of atoms in the simulation domain (from 4500 till 40500 in this study) and N_{WF} the number of Wannier functions describing the properties of each atom (N_{WF}=3 for the S atoms, 5 for the Mo, and 6 for the Ti). The momentum (k_z) dependence arises from the modeling of the out-of-plane direction z in Fig. S3, which is assumed periodic. The diagonal matrix E contains the electron energy. The block tri-diagonal matrix $\mathbf{H_{MLWF}}(k_z)$ is the k_z-dependent device Hamiltonian expressed in a MLWF basis. Finally, open boundary conditions that allow for electron injection are calculated as proposed in Ref.[7] and cast into the $\Sigma^{R,\gtrless B}(k,E)$ self-energies, while the considered scattering mechanisms, if any, are taken into account in the $\Sigma^{R,\gtrless S}(k,E)$ matrices.

As shown in Ref.,[6] the ballistic limit of transport does not capture well the physics of most 2-D materials as it neglects important conduction channels. To address this issue, it was found that introducing an energy relaxing mechanism could be really beneficial, for example, by adding (pseudo) electron-phonon interactions via the $\Sigma^{R,\gtrless S}(k,E)$ self-energies. The following expression

was considered in this work:

$$\Sigma^{\lessgtr S}(k_z,E) = \sum_{\omega_i}\int \frac{dq_z}{2\pi} M^2_{e-ph,i}\Big(n_{\omega_i} G^{\lessgtr}(k_z-q_z,E+\hbar\omega_i)+ (n_{\omega_i}+1)G^{\lessgtr}(k_z-q_z,E-\hbar\omega_i)\Big). \quad (3)$$

In Eq. (3), instead of a very accurate model, we opted for a phenomenological one where two parameters can be freely chosen, the phonon frequencies ω_i and the interaction strengths $M_{e-ph,i}$. Here, we used a single phonon energy with $\hbar\omega$=40 meV and M_{e-ph}=55 meV, which ensures a proper transfer of electrons from the Ti electrode into the MoS_2 layer. Since the scattering self-energy in Eq. (3) depends on the Green's Functions in Eqs (1)-(2) and vice-versa, these quantities must be iteratively computed within the so-called self-consistent Born approximation till convergence is reached. To obtain a conserved current, as shown in Figs. 4(b) and (e) of the main article, more than 100 Born iterations were typically required, generating a high computational burden, even on supercomputers such as the GPU-equipped Cray-XC50 Piz Daint used in this paper [1].

Finally, note that Eqs (1), (2), and (3) must be solved for all possible energy-momentum (E,k_z) pairs, i.e. for all energies where electrons are occupied and for $-\pi/L_z \leq k_z \leq \pi/L_z$, where L_z is the width of the periodic unit cell along the z direction. Due to the size of the largest investigated structures (40500 atoms) and the number of required Born iterations for current convergence ($>$100), it was not possible to account for more than one k_z point per simulation. We therefore chose a momentum with a representative current flow (based on ballistic simulations), k_z=0.7π/L_z, and restricted our calculations to it. For its part, the energy vector was discretized with a constant separation dE=0.2 meV between two adjacent points, resulting into close to 10000 energy values.

Contour Plot of the Spectral Current

To plot the spectral currents in Figs. 4(c) and (f) of the main article, the "contourf.m" function of matlab was used. As the computed data was not smooth enough to produce a clean figure with

[1] https://www.cscs.ch/computers/piz-daint/

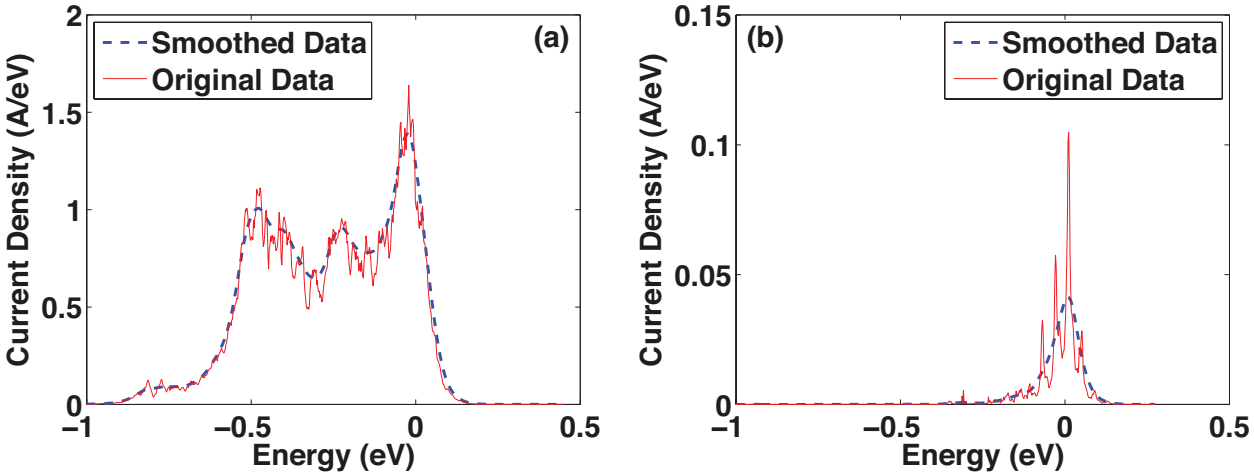

Figure S5: (a) Energy-resolved electrical current in the Ti-only region of the Ti-MoS_2 contact structure. The computed data (solid red line) and the same data after a convolution with a Gaussian function of width σ=20 meV (dashed blue cure) are plotted. The smoothed blue curve corresponds to the cut line x=0 in Fig. 4(c) of the main article. (b) Same as (a), but for the Ti-TiO_2-MoS_2 structure. The smoothed blue curve is identical to the cut line x=0 in Fig. 4(f).

all current features clearly visible, it was first convoluted with a Gaussian function to eliminate the peaks it exhibits. Figure S5 shows how the convolution modifies the data and makes it more suitable for the "contourf.m" function (no abrupt variations, while keeping the same shape).

References

(1) Szabo, A. Dissipative quantum transport simulations in two-dimensional semiconductor devices from first principles. Ph.D. thesis, ETH Zürich, 2016.

(2) Kresse, G.; Furthmüller, J. *Phys. Rev. B* **1996**, *54*, 11169–11186.

(3) Kang, J.; Sarkar, D.; Liu, W.; Jena, D.; Banerjee, K. *Proceedings of the 2012 International Electron Devices Meeting* **2012**, 17.4.1–17.4.4.

(4) Grimme, S.; Antony, J.; Ehrlich, S.; Krieg, H. *The Journal of Chemical Physics* **2010**, *132*, 154104.

(5) Mostofi, A. A.; Yates, J. R.; Lee, Y.-S.; Souza, I.; Vanderbilt, D.; Marzari, N. *Computer Physics Communications* **2008**, *178*, 685 – 699.

(6) Szabó, A.; Rhyner, R.; Luisier, M. *Phys. Rev. B* **2015**, *92*, 035435.

(7) Luisier, M.; Schenk, A.; Fichtner, W.; Klimeck, G. *Phys. Rev. B* **2006**, *74*, 205323.